Journal of the Serbian Chemical Society
JSCS-info@shd.org.rs • www.shd.org.rs/JSCS
J. Serb. Chem. Soc. 84 (11) 1329–1344 (2019)
JSCS–5267
UDC 546.62'831–19+544.654.2:549.456.4:544.032.4
Original scientific paper

Aluminum/zirconium alloys obtained by Al underpotential deposition onto Zr from low temperature $AlCl_3$+NaCl molten salts•

VESNA S. CVETKOVIĆ[1#], NIKO JOVIĆEVIĆ[2], NATAŠA M. VUKIĆEVIĆ[1#] and JOVAN N. JOVIĆEVIĆ[1*]

[1]*Institute of Chemistry, Technology and Metallurgy, University of Belgrade, Njegoševa 12, 11001 Belgrade, Serbia and* [2]*Nissan Technical Center North America, Inc.39001 Sunrise Drive, Farmington Hills, MI 48331-3487, USA*

(Received 20 June, revised 9 July, accepted 11 July 2019)

Abstract: Contrary to the widely accepted hypothesis that it is not possible, aluminum underpotential deposition (UPD) onto zirconium from a low temperature (200, 250 and 300 °C) equimolar chloroaluminate melt was recorded. Furthermore, it was shown that aluminum UPD facilitates alloy formation between the deposited aluminum monolayer and the zirconium substrate by interdiffusion. The aluminum/zirconium alloys formed at temperatures substantially lower than those needed for thermal preparation of the same alloys were Al_3Zr_2 and Al_3Zr. The experimental techniques linear sweep voltammetry, potential step, scanning electron microscopy, energy dispersive spectroscopy and X-ray diffraction were used for the characterization of the obtained electrode surfaces.

Keywords: electrochemical metal deposition; chloroaluminate melt; solid state interdiffusion; intermetallics.

INTRODUCTION

Developments of various technologies over the last few decades have resulted in an increased demand for aluminum/transitional metal alloys. Among them, Al/Mn, Al/Ti, Al/V, Al/Cr, Al/Zr and others show promise for industrial application.[1] The specific characteristics of aluminum, such as corrosion resistivity, low toxicity and relatively low price, make it a very compelling choice as the base or an alloying component for alloys.

* Corresponding author. E-mail: matori47@hotmail.com
# Serbian Chemical Society member.
• In memory of Professor Konstantin Popov who passed away in January 2019. This work is dedicated to the recognition of his outstanding contribution to the knowledge of electrochemical metal deposition.
https://doi.org/10.2298/JSC190620073C

Al/Zr alloys rich in zirconium are already used as getters for the adsorption and extraction of gases in spaces under vacuum. One of most used among them is St.101, which consists of 84 % Zr and 16 % Al, that within the working temperature range (200–450 °C) successfully absorbs all atmospheric gases.[2] Zr addition also influences the electric conductivity of Al alloys[3] and the tensile properties of some alloys at higher temperatures.[2] 6061 T6 alloy (Al–Mn–Fe–Si) has found application in the production of professional bicycle frames, which when alloyed with Zr (less than 1 at. %), saw a five-fold increase in fatigue resistance. The addition of Zr to alloys of the AA3003 (Al–Mn–Fe–Si) type has the same influence through segregation of small deposits made of Al_3Zr particles that influence alloy recrystallization, which leads to an increase of microhardness.[4,5] New lithographic plates made of at least 99.5 at. % Al, as usual, but with 0.02––0.2 at. % Zr show four times greater effectiveness at working temperatures of 320 °C than the ones with no Zr present.

Electrodeposition as a method to obtain alloys has yielded good results. However, in the case of aluminum alloys with transition metals, one has to take into account the well-known fact that Al and many other transition metals cannot be electrodeposited from aqueous solutions because hydrogen is generated before they are deposited. Therefore, a number of non-aqueous media, including inorganic molten salts, aromatic hydrocarbons, etheric solvents and ionic liquids, have been studied as potential electrolytes. Chloroaluminate molten salts, based on $AlCl_3$ mixed with an inorganic chloride salt, such as NaCl (at ≈170 °C) or an organic chloride salt, such as 1-(1-butyl) pyridinium chloride or 1-ethyl-3-methylimidazolium chloride (at close to room temperature), were also investigated as media for aluminum electrodeposition.[6,7]

Electrodeposition of metals, in general, occasionally includes underpotential deposition of the metal as well.[8–10] The phenomenon of underpotential deposition (UPD) is described as the deposition of a metal onto another metal at a potential more positive than the reversible potential of the depositing metal. The result, in principle, should be a monolayer of the depositing metal on top of another metal. In 1974, Gerischer, Kolb and Przasnyski[11–13] put forward the hypothesis to explain the origins of UPD. They claimed that in order for an underpotential deposition to appear, for a pair made of any two metals, there should exist a work function difference between the substrate metal (Φ_S) and the deposited metal (Φ_D) and it has to be negative. Soon thereafter, the formation of aluminum alloys by interdiffusion between the underpotential atomic monolayer and the substrate became obvious in the examples observed in melt-electrolytes at elevated temperatures.[9,14–21]

Published works on the electrodeposition of Al/Zr alloys are rare. Kawase *et al.* reported the electrodeposition of Al/Zr alloy films onto a carbon-coated ceramic substrate from LiCl–KCl eutectic molten salts at 550 °C.[22] Tsuda *et al.*

electrodeposited Al/Zr alloys onto Cu wire from aluminum chloride+1-ethyl-3--methylimidazolium chloride melt at 80 °C.[7] There is also an example of Al/Zr alloy coatings electrodeposited on Cu from dimethylsulfone-based baths at 110 °C by Shiomi *et al.*[23] To the best of our knowledge, aluminum electrodeposition, especially aluminum underpotential deposition, onto zirconium and subsequent Al/Zr alloy formation from a chloroaluminate eutectic mixture has not been reported except in our initial announcement.[24] The aim of the presented study was to investigate aluminum underpotential deposition onto zirconium from low temperature chloroaluminate molten salt and to establish whether an Al/Zr surface alloy was formed.

EXPERIMENTAL

All electrochemical measurements were realized in a three-electrode electrochemical cell, under an argon stream, controlled with a potentiostat/galvanostat (Princeton Applied Research, model 273A Oak Ridge, TN, USA) equipped with appropriate software (Power Suite software). Zirconium (Zr, 99.99 %; EMS Corporation, USA) wire and a planar plate were used as the working electrodes. An aluminum (Al, 99.99 %, Alfa Products, Thiokol/Ventron division, USA) rod (0.3 cm diameter) and plate (7.5 cm^2 surface area) were used as the reference and counter electrode, respectively. Before each measurement, the electrodes were polished with 0.05 μm alumina powder (Merck, Germany) and washed with deionized water. Subsequently, zirconium electrodes were etched in a solution of 50 vol % H_2O + 1 vol % HF + 1 vol % HNO_3 and the aluminum electrodes in the solutions of 50 vol % HF + 15 vol % H_2O and NH_4OH + 5 vol% H_2O_2. Finally, the electrodes were rinsed with deionized water and absolute ethanol, dried and mounted in the cell.

The procedures used for the preparation of the electrolyte – chloroaluminate molten salt and pre-electrolysis of the melt were identical to those described in a previous work.[15]

Linear sweep voltammetry (LSV) experiments were performed in the potential range starting from an initial potential, E_i (slightly negative to the zirconium reversible potential) to a final negative potential, E_f (15–100 mV negative to the aluminum reversible potential) followed by a return scan. Voltammograms recorded in the aluminum underpotential deposition range included a similar potential range scanned, except that the scan direction was changed when the potential reached E_f of 0.010 to 0.050 V positive to the aluminum reversible potential, and sometimes this E_f potential was held for τ_d of 1, 5 and 10 min. After holding, the potential was swept back to the initial potential, E_i.

Electrochemical potentiostatic deposition was realized at a constant aluminum underpotential (0.010 V) or some chosen overpotential values (–0.010 V) at three different temperatures (200, 250 and 300 °C), for 2 h, whereupon the working electrode was retrieved from the cell under potential in order to preserve deposited material or possible alloys formed. The working electrode was then washed with absolute ethanol (Zorka-Pharma, Šabac, Serbia) to remove residues of the melt, and dried in a desiccator containing silica gel. All the reported potentials of working electrodes in this work were measured relative to the equilibrium potential of the aluminum reference electrode in the melt used under the given conditions.

The morphology and composition of the deposits were analyzed by scanning electronic microscope (SEM: JEOL, model JSM-5800, Tokyo, Japan), energy dispersive spectroscopy EDS and EDX mapping (Oxford INCA 3.2, Abingdon, U.K.). After the potentiostatic electrodeposition, the Zr working electrode was examined by X-ray diffraction (XRD) on a Philips

PW 1050 powder diffractometer at room temperature with Ni-filtered CuK_α radiation (λ = = 1.54178 Å), a scintillation detector within the 15–75° 2θ range in steps of 0.05°, and scanning time of 5 s per step. The diffractograms identifying the phases formed during the deposition were compared to the recorded diffraction peaks from the Joint Committee on Powder Diffraction Standards (JCPDS) database.

RESULTS AND DISCUSSION

The potentiodynamic polarization curves (v = 1 mV s^{-1}) obtained on a zirconium electrode from equimolar $AlCl_3$+NaCl molten salt electrolyte at the different temperatures used are exhibited in Fig. 1. There are at least two apparent reversible potentials positive to the aluminum reversible potential recorded at each applied temperature. Those recorded at potentials close to the value of 0.0 V should reflect the reversible aluminum potential in the electrolyte used. However, there is at least one more reversible potential, positive to the aluminum reversible potential, which could be attributed to some phase other than metal Al being formed during the applied overpotential and underpotential regimes.

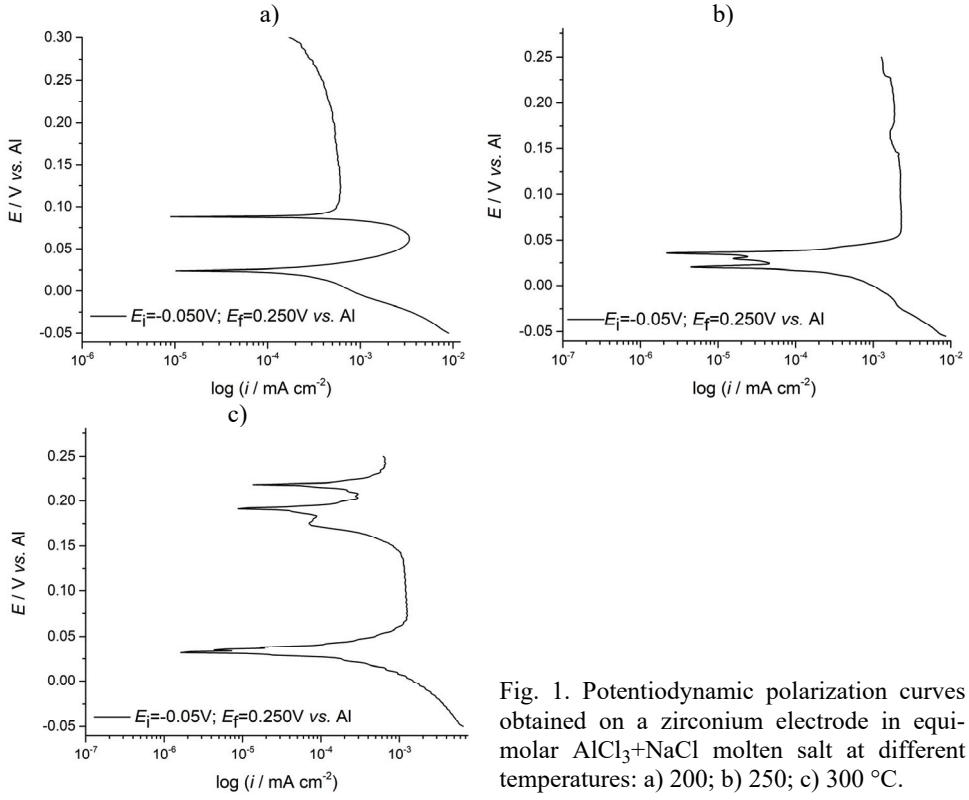

Fig. 1. Potentiodynamic polarization curves obtained on a zirconium electrode in equimolar $AlCl_3$+NaCl molten salt at different temperatures: a) 200; b) 250; c) 300 °C.

Typical voltammograms obtained from a Zr working electrode in the used melt applying different sweep rates at different temperatures in the aluminum

underpotential range are shown in Fig. 2. They show cathodic current waves with small amplitudes as well as their equally small corresponding anodic current counterparts.

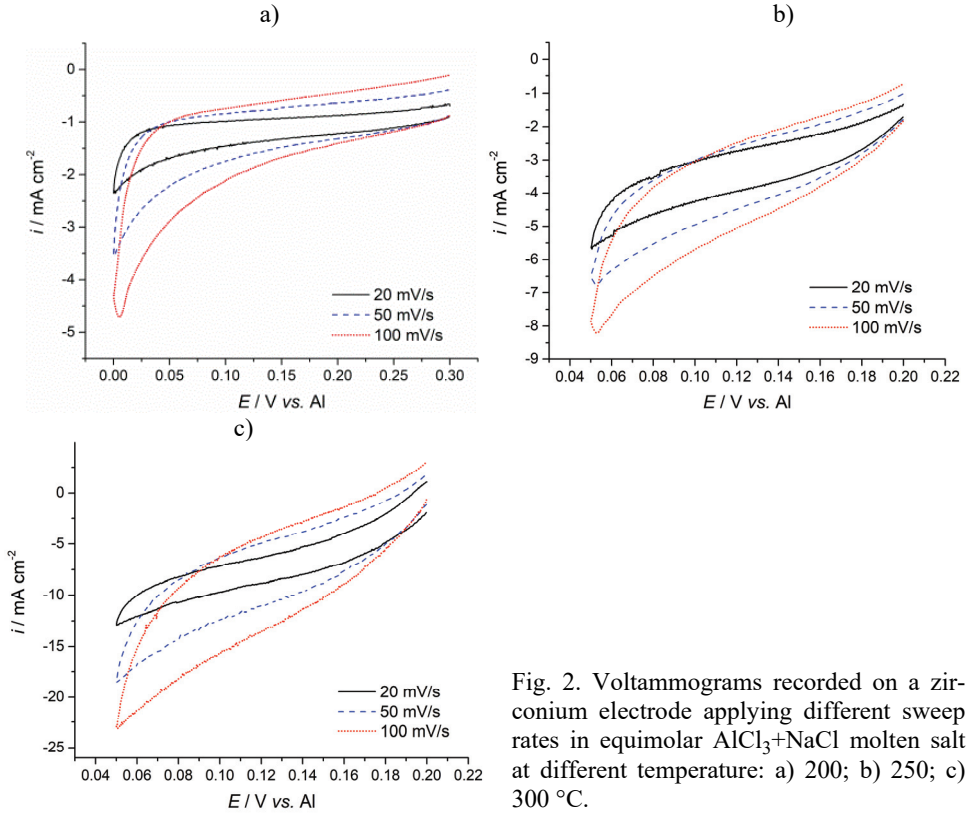

Fig. 2. Voltammograms recorded on a zirconium electrode applying different sweep rates in equimolar $AlCl_3$+NaCl molten salt at different temperature: a) 200; b) 250; c) 300 °C.

These current waves had no pronounced profiles or sharp peaks. However, a continuous increase in the reduction current as the potential was changed from 0.150 V towards 0.0 V was observed. The same was the case with the anodic current waves when the change in direction of the potential was made. The charge encompassed by the cathodic current waves and corresponding anodic current waves was similar in value and greater than the charge needed for the electrodeposition of one close-packed aluminum monolayer. Increasing the working temperature, as well as the sweep rates, induces higher current densities but does not significantly change the profiles of the curves.

Characteristic results were recorded when the LSV cycle was interrupted for a controlled period of time at the working electrode "holding potential" – E_f (the most negative potential in the cycle), Fig. 3. The current at the "holding potential", although in the Al underpotential region, increased slightly with increasing holding time, as did the subsequent corresponding dissolution charges. An inc-

rease in the working temperature, all other conditions being kept constant, led to an increase in the charge limited by the dissolution current. The anodic current waves became more pronounced and their peaks appeared at potentials similar to those indicated by the polarization curves seen in Fig. 1. In any case, the increase in the cathodic and corresponding anodic charges suggests an increase in the underpotentially deposited and dissolved aluminum.

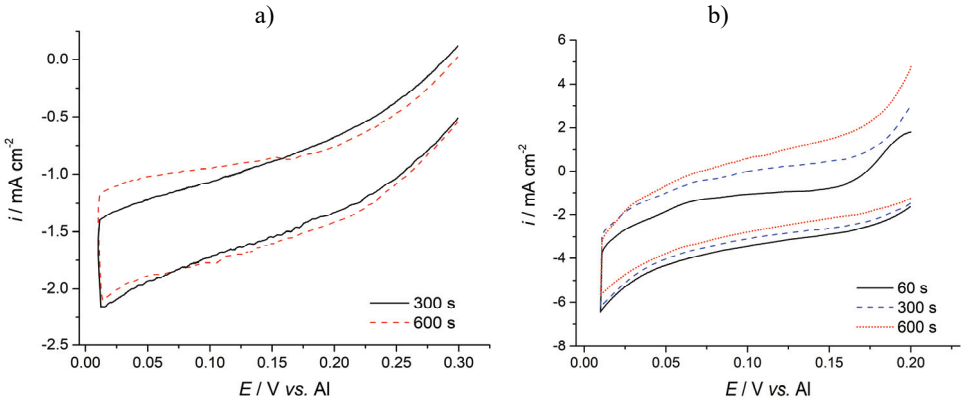

Fig. 3. Voltammograms recorded on a Zr electrode in the used melt when the cathodic end potential E_f = 0.010 V was held for different period of time; v = 10 mV s^{-1}; a) t = 200 °C; b) t = 250 °C.

The appearance of such reduction and oxidation current waves, which do not show pronounced amplitudes in voltammograms recorded in the underpotential range, are characteristic of metal underpotential deposition and dissolution in some other cases.[18,19] Those cases suggested that such voltammograms represent underpotential deposition of aluminum onto Zn and Cd substrate even though, according to Gerischer *et al.*,[11–13] underpotential deposition should not occur. Namely, half of the difference of electron functions between Al and Zn, and Al and Cd is negative or very close to zero and, as a result, there should not be a driving force for Al underpotential deposition onto Zn or Cd substrates. However, aluminum was underpotential deposited in those cases and it was always accompanied by alloy formation between the deposited Al and Cd or the Zn substrate. It appears that the Al/Zr pair in the same electrolyte and under the same temperatures used behaves very similarly to Al on Cd and Al on Zn pairs, *i.e.*, there seems to be an Al underpotential deposition onto the Zr surface, as well as Al/Zr alloy formation.

Changes of the working electrode "open circuit potential" with time after being held for 60 min at the Al underpotential of 0.020 V are presented in Fig. 4 for all three applied deposition temperatures (200, 250 and 300 °C). At least one plateau was observed at a potential different from the one reflecting aluminum or

Zr reversible potentials in the system used. The values of these plateau potentials were close to the values of the reversible potentials in the aluminum underpotential region recorded in Figs. 1a, b and c. By definition, these potentials define a phase on the electrode surface in equilibrium with its ions in the electrolyte. Since the plateau potentials are substantially more positive than the aluminum reversible potential in the system observed, they should not reflect bulk aluminum on the surface of the Zr working electrode in equilibrium with potentials of the zirconium/aluminum surface alloys made by aluminum underpotential deposition onto zirconium and subsequent interdiffusion with the substrate. This approach is supported by LSV results, Figs. 2 and 3, and agrees with findings reported elsewhere.[18,19]

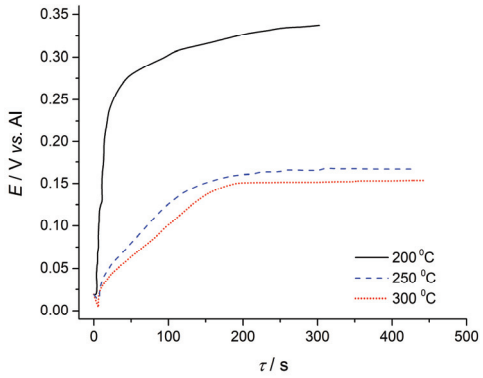

Fig. 4. Change of the working electrode "open circuit potential" recorded after the electrode had been exposed to a potential of 0.020 V for 60 min, at three different temperatures.

The results of LSV experiments with the cathodic end potential E_f being led into the aluminum overpotential region using the same sweep rate at different temperatures are presented in Fig. 5.

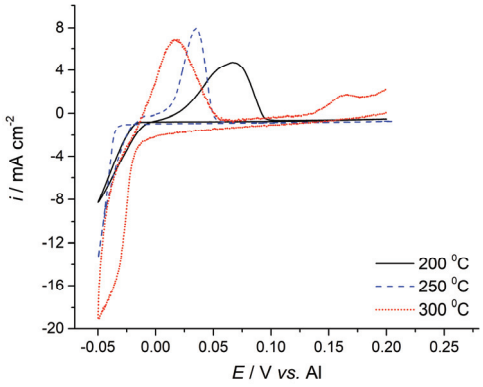

Fig. 5. Voltammograms recorded on a Zr working electrode with the cathodic end potential in the aluminum overpotential region (E_f = –0.050 V) in equimolar $AlCl_3$+NaCl melt, v = 10 mV s^{-1}.

Two features were observed: *i*) there was a current increase announcing Al bulk deposition at potentials cathodic of ≈ –0.030 V and the anodic counterpart at

potentials anodic of ≈ 0.000 V, reflecting dissolution of the deposited bulk Al; *ii*) at 250 °C, there was a hint of an anodic current increase at ≈ 0.175 V, and at 300 °C, a visible anodic current wave formed with the peak at ≈ 0.175 V. This group of second anodic current waves appeared at anodic potentials very close to those seen in Figs. 2–4, and most probably represent dissolution of the surface Zr/Al alloys formed by aluminum underpotential deposition and interdiffusion with the zirconium substrate.

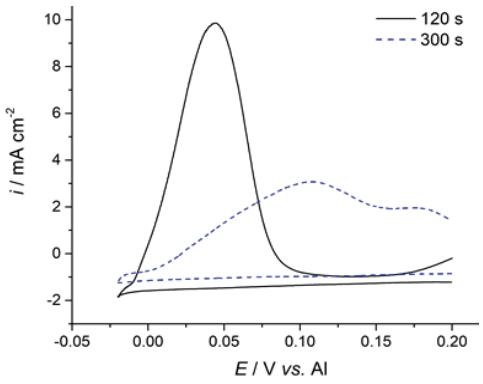

Fig. 6. Voltammograms obtained from a Zr electrode in the used electrolyte at 250 °C with different holding times at the negative end potential of the cycle, E_f.

These assumptions were supported by voltammograms obtained when the negative end potential of the cycle was held for some time in the aluminum overpotential range and then returned back to the starting potential of the cycle. The resulting large anodic dissolution current waves, the amplitude and peak number of which increased with increasing holding time of the chosen cathodic overpotential, were recorded and are presented in Fig. 6. The charge under the anodic current waves indicates dissolution of the previously deposited aluminum, but the appearance of a multipeak structure obtained with increased holding time suggests additional phase(s) being formed. The peak potential of the second anodic peak at ≈0.175 V agrees well with the anodic peak potential values seen in voltammograms Figs. 2, 3 and 5, and the plateau potential values recorded in polarization curve and open circuit measurements, Figs. 1 and 4. It could be concluded that part of the deposited aluminum enters the substrate and forms an alloy with the substrate, which is then dissolved at anodic potentials close to ≈0.175 V. The finding that this alloy dissolution peak appears at the same potentials as a result of similar experiments, Figs. 2–4, in the underpotential range, suggests Al/Zr alloy formation by Al underpotential deposition onto Zr substrate in the investigated system.

SEM, EDS and EDX analyses of the working electrode surface exposed for some time to aluminum underpotentials provided additional data on aluminum being underpotentially deposited onto zirconium substrate in the investigated system, Fig. 7. Particularly convincing were the results of EDS and EDX analysis

that not only register the presence of aluminum on the zirconium substrate after underpotential deposition, but give comparative maps of the distribution of aluminum and zirconium in the working electrode surface. The white areas in the EDX maps from Fig. 7 indicate the positions and distribution of the elements: c) zirconium, d) aluminum and e) oxygen present in the sample surface. These results conclusively confirm aluminum underpotential deposition onto zirconium proposed on the grounds of the experimental results presented in Figs. 2–6.

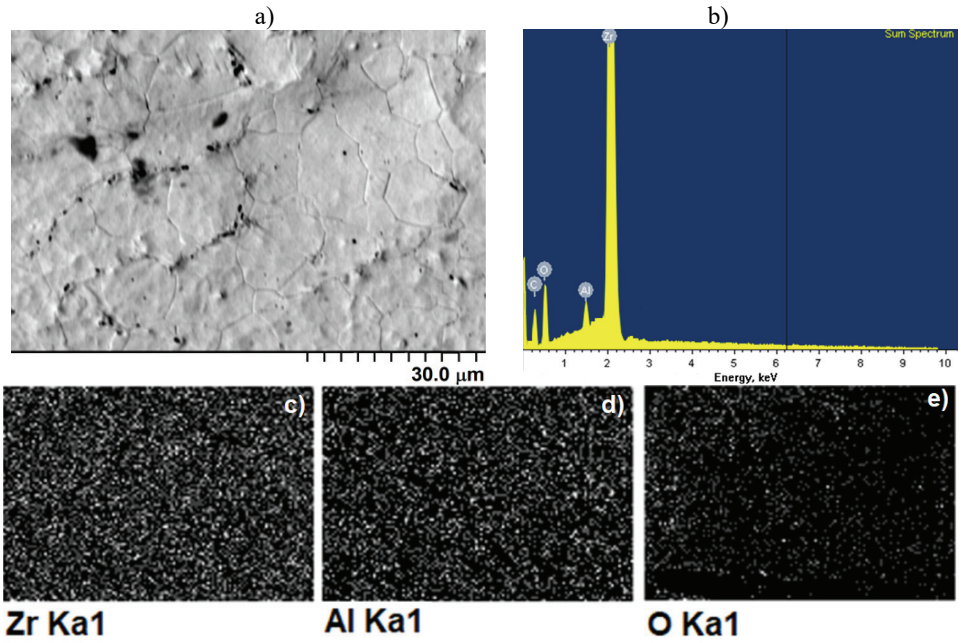

Fig. 7. a) SEM photographs of the surface of the working electrode exposed to a potential of 0.010 V for 2 h in the $AlCl_3$+NaCl melt at 250 °C, magnification 1500×; b) EDS analysis of the sample and: c), d) and e) EDX maps of the surface shown in a).

Examples of XRD diffraction patterns of zirconium substrates exposed for some time to aluminum underpotential (0.010 V) at the three chosen temperatures are exhibited in Fig. 8. Each of them indicates the presence of at least two Al/Zr alloys. The differences introduced in the XRD spectra for the substrate samples obtained at different working temperatures are shown by the different number of Al/Zr alloys formed as a result of aluminum underpotential deposition in the investigated system. No spectrum for bulk aluminum was recorded. The Al_3Zr alloy was present in the substrate surface irrespective of the working temperature after aluminum underpotential deposition. The same alloy was the only one formed during overpotential Al deposition, see Fig. 9. This implies that the significant supply of aluminum to the substrate surface, compared to underpot-

ential deposition, continue to favor the formation of what seems to be the alloy with the lowest energy of formation for the governing conditions in all the investigated systems.

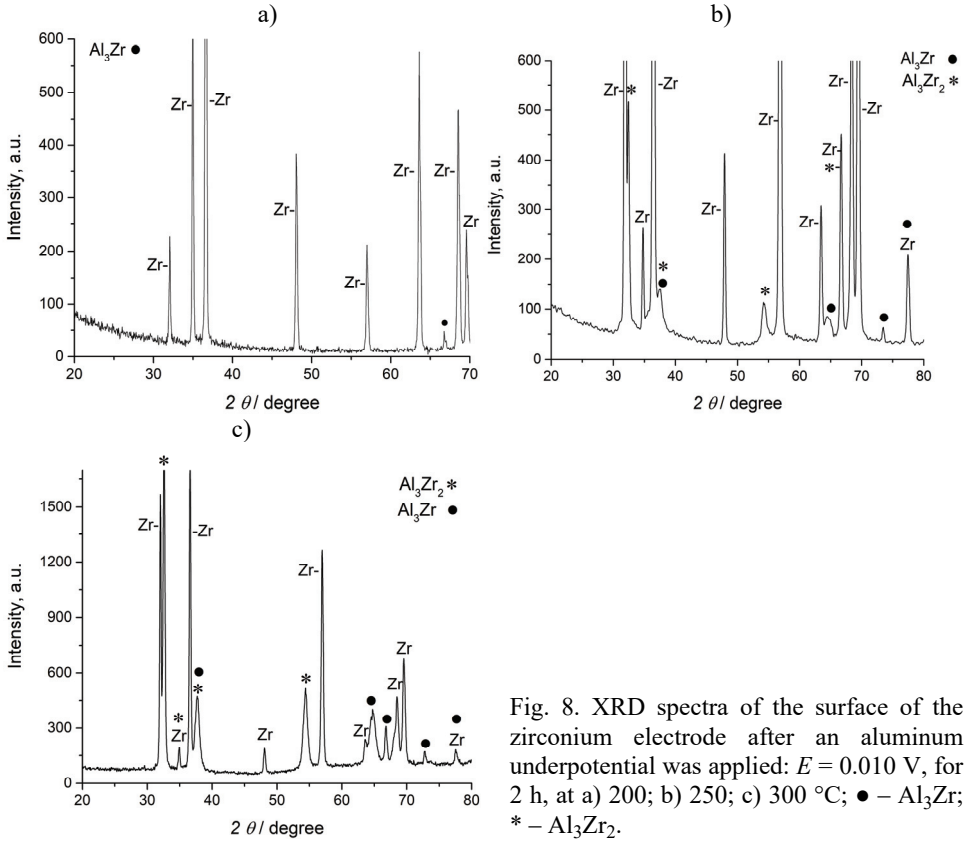

Fig. 8. XRD spectra of the surface of the zirconium electrode after an aluminum underpotential was applied: E = 0.010 V, for 2 h, at a) 200; b) 250; c) 300 °C; ● – Al_3Zr; * – Al_3Zr_2.

Final evidence of aluminum underpotential deposition and alloy formation with the zirconium substrate in the chosen system under the chosen temperatures and other conditions were provided by XRD analysis of the working electrodes after prolonged time spent under the investigated aluminum underpotential, Fig. 8.

Formation of the first aluminum monolayer onto zirconium surface is followed by diffusion of aluminum atoms into the substrate, the alloying process being continuously supplied with material by newly underpotentially deposited aluminum.

The results obtained in the present investigation of underpotential aluminum electrodeposition onto zirconium from equimolar $AlCl_3$+NaCl melt at 200, 250 and 300 °C can nominate the formation of the following Al/Zr alloys:

- orthorhombic Al_3Zr_2, most intensive 2θ values: 32.91, 34.68, 37.33, 54.04, 54.28 and 67.15° (JCPDS No. 00-048-1383);
- tetragonal Al_3Zr, most intensive 2θ values: 27.35, 38.08, 53.95, 63.34, 65.86, 73.79 and 78.82° (JCPDS No. 00-048-1385).

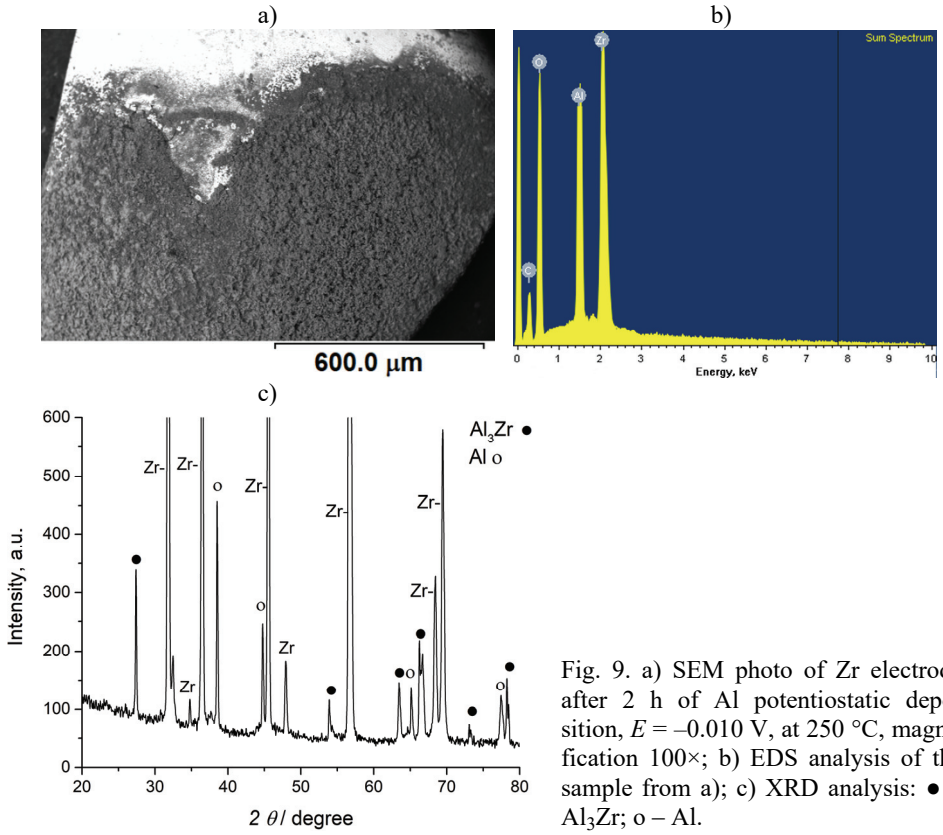

Fig. 9. a) SEM photo of Zr electrode after 2 h of Al potentiostatic deposition, E = –0.010 V, at 250 °C, magnification 100×; b) EDS analysis of the sample from a); c) XRD analysis: ● – Al_3Zr; o – Al.

In discussing the possibility of Al/Zr alloy formation, one should bear in mind that among all the binary phase diagrams of aluminum with transition metals, the Al–Zr diagram is one of the most complex.[25,26] It consists of ten recognized compounds of different concentrations, each of which appears in a narrow concentration band (most often in the order of 1 at. %). Two of the phases (namely Zr_5Al_3 and Zr_5Al_4) are high temperature phases while the rest of the phases decompose and transform into other phases at higher temperatures. Most of the phases appear in hexagonal, orthorhombic, tetragonal and cubic structures and four of them appear in new prototype forms. Maximum solubility of aluminum in zirconium is 26 at. % at 1350 °C.

It should be noted that a detailed review of the available literature did not provide reports on electrodeposition of aluminum onto zirconium from inorganic melts or ionic solutions either by underpotential or overpotential electrodeposition to compare the present results with.

Meanwhile, the last twenty years have seen several published works[7,23,27] on the subject of the electrolytical co-deposition of zirconium and aluminum from ionic solutions. In one of these papers,[7] the authors elaborate on the dependence of the structure of the Al/Zr alloy deposited on the chemical composition and temperature, and concluded that zirconium practically does not dissolve in fcc aluminum at room temperature. However, they found that metastable solid-state Al/Zr solutions show good thermal stability up to 400–450 °C. They explain that the thermal decomposition of a saturated solid-state solution leads to nucleation of the metastable Al_3Zr phase ordered into a cubic LI_2 structure or to an equilibrated Al_3Zr phase of tetragonal structure. Alloys with a higher Zr content (up to 16.6 at. %) should be entirely amorphous. Such two-phase regions are common among alloys obtained by the co-deposition of aluminum with transition metals when the concentration of the transition metal exceeds the saturation limit of the solid solution fcc structure in Al.

However, there is literature that reports on developments in physical manufacturing methods designed around the intimate contact of aluminum and zirconium thin layers, which to some extent resemble the interface studied in the present work. There are examples where thin films of aluminum and zirconium, made by vacuum vapor deposition brought into contact at a temperature between 553 and 640 °C show alloy formation by interdiffusion.[28,29] In such cases, only one intermediate phase was formed, namely Al_3Zr. The authors proposed a sequence of events in the diffusion zone of the process leading to the formation of the said alloy:

a) saturation of the initial solution with atoms of the solute,
b) nucleation of the intermediate phase (Al_3Zr), and
c) growth of the newly formed phase.

At 600 °C, the solubility of Zr in Al is only 0.07 at. % and of Al in Zr, it is 1.2 at. % and so it should be expected that the initial solid solution will be saturated first with aluminum.

The ease with which the nucleation of the Al_3Zr phase proceeds next to the aluminum surface could be explained by the structure of its lattice. Aluminum crystallizes as a fcc lattice with a first neighbor atomic distance of 2.86 Å. Al_3Zr is a body centered tetragonal lattice of the DO_3 type and it could be easily considered as a slightly deformed modification of a fcc structure. In the Al_3Zr structure, the Al–Al distance is 2.80 and 2.85 Å, which approaches the value of pure Al. It is obvious that orderly incorporation and positioning of Zr atoms into the Al atom matrix leads to the formation of Al_3Zr without significant strain energy.

The high formation rate of Al_3Zr compared to other phases is most probably the result of the relatively large diffusion coefficients of Zr and Al in that phase. This suggests that concentration gradients are being formed through the defective lattice as a result of increased concentration of vacancies (positions not occupied by Al atoms in the Al_3Zr lattice). Each Al atom has eight Al and four Zr positions in its coordination shell. Simultaneously, a Zr atom is completely surrounded only by Al positions. As a consequence, free Al positions, which are in principle available to both Al and Zr atoms, will more probably be exchanged with an Al atom then with a Zr atom because the latter has to overcome a lattice order barrier in addition to the normal barrier needed to attain an Al position. For this reason, the Zr diffusion coefficient through the Al_3Zr phase is smaller than for Al.

A previous work[30] that elaborates on mechanical Al/Zr alloying of two metal powders at room temperature agree with the above approach to zirconium being alloyed by the diffusion of aluminum. During mechanical mixing (a mill with balls) of Al and Zr powders, the Zr grains become covered with an Al layer. Due to further friction, the Al layer dissolves and incorporates into the Zr structure by diffusion because of the high negative enthalpy of mixing between Al and Zr. This leads to the formation of an Al concentration profile in Zr and to appropriate changes of the lattice parameters followed by a metastable disordered solid state solution. When the Al concentration in Zr increases over 15 at. % (up to 40 at. % Al), the hexagonal Zr structure becomes unstable and transforms into a glassy structure (amorphous phase of Zr_3Al). Above 50 at. % Al, the metastable face centered cubic lattice of the ZrAl phase is formed.

In another work,[31] the authors pressed nanocrystalline powders of Al and Zr at 76 to 100 °C and analyzed the obtained Al/Zr alloy at room temperature. They found that even in the alloy made of 5–35 mas. % Zr, the metastable cubic Al_3Zr LI_2 phase was observed, which appears in processes of abrupt solidification. This was contrary to the Al–Zr phase diagram that proposes the coexistence of Al with changing quantities of $ZrAl_3$ of DO_{23} phase. The assumption was that nucleation of simple Li_2 cell requires less energy than the bigger and more complex DO_3 structure. Smaller particles are more reactive and prone to higher diffusion rates, which reduces the nucleation barrier of the LI_2 phase.

Recently, a number of reports appeared[32–36] which analyzed the formation of alloys by interdiffusion between zirconium and aluminum thin films, deposited onto silicon or graphite by magnetron spattering. These films were heated at temperatures from 100 to 700 °C for one hour. It was established that interdiffusion between the films starts above 200 °C. The first visible changes in the structure of the multilayer system appeared at 250 °C followed by an increase in the interdiffusion rate and initiation of mixing of the Zr and Al layers into an amorphous alloy. At 290 °C, the interface consists of an amorphous Zr/Al alloy

and a cubic Al_3Zr alloy. Above 295 and 298 °C, the interface phase alloys transform completely into a polycrystalline mixture of hexagonal close packed $ZrAl_2$ and cubic Al_3Zr.

CONCLUSIONS

Half of the difference between work functions of zirconium and aluminum is small and negative. Thus according to the Gerischer–Kolb hypothesis,[9–11] there should be no underpotential deposition of aluminum onto zirconium.

However, the present experiments of aluminum deposition onto zirconium from equimolar chloraoaluminate melts at potentials positive to the aluminum reversible potential performed at 200, 250 and 300 °C revealed underpotential deposition of aluminum, resulting in the formation of Al/Zr surface alloys formation. The alloys recorded were Al_3Zr_2 and Al_3Zr.

The alloys were formed at temperatures several hundred degrees lower than the temperatures needed for the production of the same alloys by thermal processes.

ИЗВОД

ЛЕГУРЕ АЛУМИНИЈУМА И ЦИРКОНИЈУМА ДОБИЈЕНЕ ЕЛЕКТРОХЕМИЈСКИМ ТАЛОЖЕЊЕМ АЛУМИНИЈУМА ПРИ ПОТПОТЕНЦИЈАЛУ НА ЦИРКОНИЈУМУ ИЗ НИСКОТЕМПЕРАТУРНИХ $AlCl_3$+NaCl РАСТОПА

ВЕСНА С. ЦВЕТКОВИЋ[1], НИКО ЈОВИЋЕВИЋ[2], НАТАША М. ВУКИЋЕВИЋ[1] и ЈОВАН Н. ЈОВИЋЕВИЋ[1]

[1]ИХТМ – Центар за електрохемију, Универзитет у Београду, Његошева 12, Београд и [2]Nissan Technical Center North America, Inc.39001 Sunrise Drive, Farmington Hills, MI 48331-3487, USA

Насупрот широко прихваћеној хипотези по којој то није вероватно, установљено је постојање електрохемијског таложења алуминијума при потпотенцијалу на цирконијуму из нискотемпературног (200, 250 и 300 °C) еквимоларног хлороалуминатног растопа. Надаље, показано је да електрохемијско таложење алуминијума при потпотенцијалу омогућава формирање легура између исталоженог монослоја алуминијума и цирконијумове подлоге путем интердифузије. Легуре алуминијума и цирконијума Al_3Zr_2 и Al_3Zr формиране су на температурама које су значајно мање од оних потребних за термичко припремање таквих легура. Коришћене експерименталне технике биле су линеарне цикличка волтаметрија и потенциостатски пулс, скенирајућа електронска микроскопија, енергетско дисперзивна спектроскопија и дифракција X-зрака коришћене су за карактеризацију добијене електродне површине.

(Примљено 20. јуна, ревидирано 9 јула, прихваћено 11. јула 2019)

REFERENCES

1. M. Ueda, *J. Solid State Electrochem.* **21** (2017) 641 (http://dx.doi.org/10.1007/s10008-016-3428-8)
2. G. Garza-Elizondo, S. Alkahtani, A. Samuel, F. Samuel, in *Light Metals 2014*, J. Grandfield, Ed., Springer International Publishing, Cham, 2016, pp. 305–314 (http://dx.doi.org/10.1007/978-3-319-48144-9)
3. T. Knych, M. Piwowarska, P. Uliasz, *Arch. Metall. Mater.* **56** (2011) 685 (http://dx.doi.org/10.2478/v10172-011-0075-z)
4. M. Pokova, M. Cieslar, J. Lacaze, in *Met. 2012 Conf. Proc.*, Brno, 2012, pp. 1149–1155

5. M. Pokova, M. Cieslar, P. Malek, in *Met. 2013 Conf. Proc.*, Brno, Czech Republic, 2013
6. M. Ueda, T. Teshima, H. Matsushima, T. Ohtsuka, *J. Solid State Electrochem.* **19** (2015) 3485 (http://dx.doi.org/10.1007/s10008-015-2861-4)
7. T. Tsuda, C. L. Hussey, G. R. Stafford, O. Kongstein, *J. Electrochem. Soc.* **151** (2004) C447 (http://dx.doi.org/10.1149/1.1753231)
8. E. Budevski, G. Staikov, W. J. Lorenz, *Electrochemical Phase Formation and Growth: an introduction to the initial stages of metal deposition*, Wiley-VCH, New York, 1996
9. G. R. Stafford, C. L. Hussey, in *Adv. Electrochem. Sci. Eng.*, R. C. Alkire, D. M. Kolb, Eds., Wiley-VCH, New York, Weinheim, 2001, pp. 275–348
10. A. Oveido, L. Reinaudi, S. G. Garcia, E. P. M. Levia, *Underpotential Deposition: From fundamentals and theory to aplications at the nanoscale*, Springer International Publishing, Cham, 2016 (http://dx.doi.org/10.1007/978-3-319-24394-8)
11. D. M. Kolb, M. Przasnyski, H. Gerischer, *Electroanal. Chem. Interfacial Electrochem.* **54** (1974) 25
12. H. Gerischer, D. M. Kolb, M. Przasnyski, *Surf. Sci.* **43** (1974) 662
13. D. M. Kolb, H. Gerischer, *Surf. Sci.* **51** (1975) 323
14. V. D. Jović, J. N. Jovićević, *J. Appl. Electrochem.* **19** (1989) 275 (http://dx.doi.org/10.1007/BF01062312)
15. B. Radovic, R. A. H. Edwards, V. S. Cvetković, J. N. Jovicevic, *Kov. Mater.* **48** (2010) 55 (http://dx.doi.org/10.4149/km_2010_1_55)
16. B. S. Radović, V. S. Cvetković, R. A. H. Edwards, J. N. Jovićević, *Kov. Mater.* **48** (2010) 159 (http://dx.doi.org/10.4149/km_2010_3_159)
17. B. S. Radović, V. S. Cvetković, R. A. H. Edwards, J. N. Jovićević, *Int. J. Mater. Res.* **102** (2011) 59 (http://dx.doi.org/10.3139/146.110443)
18. N. Jovićević, V. S. Cvetković, Ž. J. Kamberović, J. N. Jovićević, *Int. J. Electrochem. Sci.* **7** (2012) 10380
19. N. Jovićević, V. S. Cvetković, Ž. J. Kamberović, J. N. Jovićević, *Metall. Mater. Trans., B: Process Metall. Mater. Process. Sci.* **44** (2013) 106 (http://dx.doi.org/10.1007/s11663-012-9750-3)
20. N. Jovićević, V. S. Cvetković, Ž. Kamberović, T. S. Barudžija, *Int. J. Electrochem. Sci.* **10** (2015) 8959
21. V. S. Cvetković, L. Bjelica, N. M. Vukićević, J. N. Jovićević, *Chem. Ind. Chem. Eng. Q.* **21** (2015) 527 (http://dx.doi.org/10.2298/CICEQ141205009C)
22. M. Kawase, Y. Ito, *J. Appl. Electrochem.* **33** (2003) 785 (http://dx.doi.org/10.1023/A:1025513222091)
23. S. Shiomi, M. Miyake, T. Hirato, *J. Electrochem. Soc.* **159** (2012) D225 (http://dx.doi.org/10.1149/2.079204jes)
24. V. S. Cvetković, N. Jovićević, N. M. Vukićević, , in *Proceedings of 49th Int. Oct. Conf. Min. Metall.*, N. Štrbac, I. Marković, L. Balanović, Eds., University of Belgrade, Technical Faculty in Bor, Bor, Serbia, 2017, pp. 241–244
25. J. Murray, A. Peruzzi, J. P. Abriata, *J. Phase Equilibria* **13** (1992) 277 (http://dx.doi.org/10.1007/BF02667556)
26. M. Alatalo, M. Weinert, R. E. Watson, *Phys. Rev., B* **57** (1998) R2009
27. A. Stakėnas, L. Simanavièius, *Chemistry (Vilnius)* **12** (2001) 189
28. G. V. Kidson, G. D. Miller, *J. Nucl. Mater.* **12** (1964) 61 (http://dx.doi.org/10.1016/0022-3115(64)90108-4)
29. K. E. Knipling, D. C. Dunand, D. N. Seidman, *Acta Mater.* **56** (2008) 114 (http://dx.doi.org/10.1016/j.actamat.2007.09.004)

30. H. J. Fecht, G. Han, Z. Fu, W. L. Johnson, *J. Appl. Phys.* **67** (1990) 1744 (http://dx.doi.org/10.1063/1.345624)
31. M. N. Rittner, J. R. Weertman, J. A. Eastman, *Acta Mater.* **44** (1996) 1271 (http://dx.doi.org/10.1016/1359-6454(95)00303-7)
32. J. Ho, K. Lin, *J. Appl. Phys.* **75** (1994) 2434 (http://dx.doi.org/10.1063/1.356267)
33. I. L. Soroka, J. Vegelius, P. T. Korelis, A. Fallberg, S. M. Butorin, B. Hjörvarsson, *J. Nucl. Mater.* **401** (2010) 38 (http://dx.doi.org/10.1016/j.jnucmat.2010.03.016)
34. J. Vegelius, I. L. Soroka, P. T. Korelis, B. Hjörvarsson, S. M. Butorin, *J. Phys. Condens. Matter* **23** (2011) 265503 (http://dx.doi.org/10.1088/0953-8984/23/26/265503)
35. Q. Zhong, Z. Zhang, J. Zhu, Z. Wang, P. Jonnard, K. Guen, Y. Yuan, J.-M. André, H. Zhou, T. Huo, *Appl. Phys. A* **109** (2012) 133 (http://dx.doi.org/10.1007/s00339-012-7085-1)
36. Q. Zhong, Z. Zhang, S. Ma, R. Qi, J. Li, Z. Wang, P. Jonnard, K. Le Guen, J.-M. André, *Appl. Surf. Sci.* **279** (2013) 334 (http://dx.doi.org/10.1016/j.apsusc.2013.04.094).